Application of a sunburst aperture to diffraction suppression*

B. K. Yap and S. D. Fantone

Honeywell Radiation Center, Honeywell, Inc., 2 Forbes Road, Lexington, Massachusetts 02173

(Received 25 January 1974)

A closed-form solution to a two-dimensional Fourier transform of a toothed wheel or sunburst is presented. The solution was obtained by decomposing the sunburst aperture into triangles and applying the superposition principle to sum the Fourier transforms of the subapertures. This technique is applicable to analyzing and designing other complicated apertures. Computer plots are presented that show the spatial transforms along the radial and angular directions. For small radial distances, the transform resembles that of a circle, whereas for large radial distances, it has preferred angular directions that are perpendicular to every edge of the aperture. The power spectrum or the magnitude squared of the transform is a close approximation of the Fraunhofer diffraction pattern of the aperture. Contour shaping of this type is an effective means of apodizing diffraction of unwanted sources of small angular subtense but becomes ineffective when the angular subtense of the unwanted sources are large.

Index Headings: Diffraction; Fourier transforms.

Optical-sensor sensitivities are limited by noise generated both within and outside of the system. Within the sensor, noise sources could be mechanical, optical, or electronic, whereas noise generated exterior to a properly electronically shielded system may be coupled into the sensor only optically. One such instance is a solar coronograph, which in general is limited by the solar irradiance outside the field of view, scattered or diffracted onto the axis. Scattering may be suppressed by use of highly polished homogeneous optical elements, blackening of optical housing, and reduction of aerosol within the instrument. Diffraction is due to the finite sizes of the optical elements which cause distortions of the input wave front, resulting in deviations from rectilinear propagation. The effects of diffraction may be reduced by proper design and location of stops as well as by apodizing the optical elements. Apodization by use of a transmission filter has been studied in great detail by Jacquinot[1] and found to be effective in suppressing the wings of the diffraction pattern. Contour shaping has had attention in recent years[2,3] as an alternative method of reducing the effects of diffraction without significant loss of optical efficiency, but success has been limited.

OFF-AXIS REJECTION

One type of contour shaping in particular is investigated here and evaluated for effectiveness in rejection of diffracted light from unwanted sources. The requirements for suppression of stray light depend on the source characteristics, i.e., source emissions, reflections, spectral distribution, and angular subtense. The capability of the system to reject stray light may be characterized by its point-source rejection, which is defined as

$$R_{ps}(\phi) = \frac{\text{power at detector with point source off axis}}{\text{power at detector with point source on axis}}. \quad (1)$$

It is, in general, a function of off-axis angle ϕ and, in cases in which there is not circular symmetry, also a function of θ, angular direction in a plane perpendicular to the optical axis. This is analogous to the point spread function. Convolution of $R_{ps}(\phi)$ with the source function yields the stray light per unit collecting aperture that enters the system. The source function is the product of the source solid-angular distribution with its radiance (watts/area/steradian). For each source function, there is a family of point-source rejection curves that would yield the same quantity of stray light.

DIFFRACTION AND FOURIER TRANSFORM

Use of Huygens–Fresnel principle for interference of light and application of Kirchhoff's boundary approximations at a diffracting aperture yields the familiar equation for the diffracted electric field[4] (see Fig. 1)

$$E(X_2,Y_2) = \frac{1}{j\lambda}\int\int \frac{E(X_1,Y_1)}{r}\cos\phi \exp\left(j\frac{2\pi r}{\lambda}\right)dx_1\,dy_1, \quad (2)$$

where $\cos\phi$ represents the projection of the diffracting incremental area onto the line of sight, r, and λ is the wavelength of the monochromatic point source. For Fraunhofer diffraction, in which cases the plane of observation is at a large distance, z, and the angle ϕ is small, the observed diffracted E field may be approximated by[4]

$$E(X_2,Y_2) = \frac{1}{j\lambda z}\exp\left[j\frac{\pi}{\lambda z}(X_2^2+Y_2^2)\right]\mathrm{FT}[E(X_2,Y_2)], \quad (3)$$

where FT denotes Fourier transform. A similar approximation is obtained for diffraction in the back focal plane of an optical element.[4] For heterochromatic sources, the observed diffraction pattern is the inte-

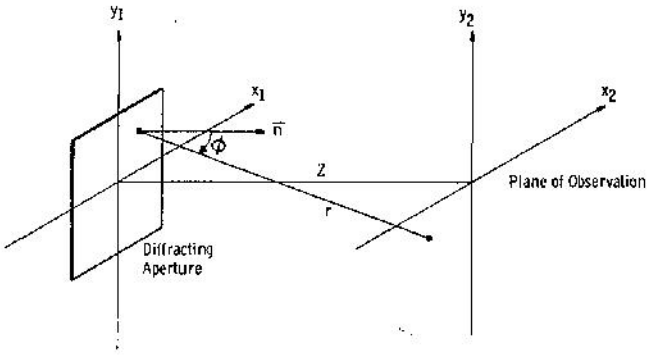

FIG. 1. Diffraction coordinate system.

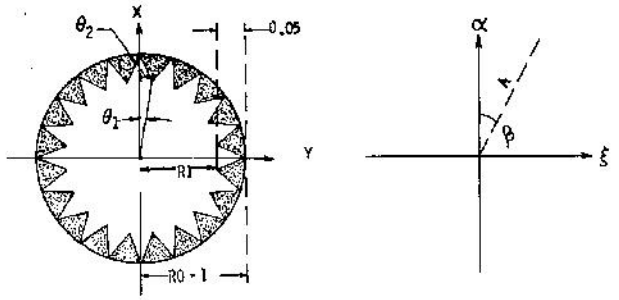

FIG. 2. Contour shaping of a circle into a sunburst aperture. Example shown with 20 teeth.

gration over wavelength of the spectral irradiance, i.e., the square of the magnitude of E. In the case of an extended source, a model may be used in which the extended source is approximated by spatially incoherent point sources; a second integration over the source function then yields the total diffracted flux. Such a treatment may be extended to include systems that consist of more than one optical element.

Equation (3) in principle, can be used to analyze and, to a certain extent, to design diffracting apertures that otherwise cannot be designed by use of the more-exact form, Eq. (2). Apertures may be dissected and summed by application of the superposition integral. Complicated apertures may sometimes by expressed in closed form by decomposing them into subapertures that have simpler configurations, such as circles, squares, triangles, and ellipses.

FOURIER TRANSFORM OF A SUNBURST

The Fourier transform of a sunburst aperture is easily calculated by decomposing the aperture into triangular sections (Fig. 2). When the transform for one radial tooth has been found, simple rotation of coordinates and summation of the contributions from all teeth yields the complete transform. The Fourier transform for a radial tooth (Fig. 2) is

$$
\begin{aligned}
F(\alpha,\xi) &= \int_{-\infty}^{\infty}\int_{-\infty}^{\infty} A(x,y)\exp\{-j2\pi(\alpha x+\xi y)\}\,dy\,dx \\
&= \int_{0}^{R1}\int_{-x\tan\theta_1}^{x\tan\theta_1} 1\exp\{-j2\pi(\alpha x+\xi y)\}\,dy\,dx + \int_{R1}^{R0}\int_{-R1(\tan\theta_1+\tan\theta_2)+x\tan\theta_2}^{R1(\tan\theta_1+\tan\theta_2)-x\tan\theta_2} 1\exp\{-j2\pi(\alpha x+\xi y)\}\,dy\,dx \\
&= \int_{0}^{R1}\exp\left\{-j2\pi\alpha x\frac{\sin(2\pi\xi x\tan\theta_1)}{\pi\xi}\right\}dx + \int_{R1}^{R0}\exp\left\{-j2\pi\alpha x\frac{\sin 2\pi\xi[R1(\tan\theta_1+\tan\theta_2)-x\tan\theta_2]}{\pi\xi}\right\}dx \\
&= F_1(\alpha,\xi)+F_2(\alpha,\xi)+F_3(\alpha,\xi), \qquad (4)
\end{aligned}
$$

where

$$
\begin{aligned}
F_1(\alpha,\xi) &= \frac{1}{\pi\xi(4\pi^2\xi^2\tan^2\theta_1-4\pi^2\alpha^2)} \\
&\quad\times[2\pi\xi\tan\theta_1-\exp\{-j2\pi\alpha R1\}[j2\pi\alpha\sin(2\pi\xi R1\tan\theta_1)+2\pi\xi\tan\theta_1\cos(2\pi\xi\tan\theta_1)]], \\
F_2(\alpha,\xi) &= \frac{\sin[2\pi\xi R1(\tan\theta_1+\tan\theta_2)]}{\pi\xi(4\pi^2\xi^2\tan^2\theta_2-4\pi^2\alpha^2)} \\
&\quad\times[\exp\{-j2\pi\alpha R0\}[-j2\pi\alpha\cos(2\pi\xi R0\tan\theta_2)+2\pi\xi\tan\theta_2\sin(2\pi\xi R0\tan\theta_2)] \\
&\quad\quad-\exp\{-j2\pi\alpha R1\}[-j2\pi\alpha\cos(2\pi\xi R1\tan\theta_2)+2\pi\xi\tan\theta_2\sin(2\pi\xi R1\tan\theta_2)]], \\
F_3(\alpha,\xi) &= -\frac{\cos[2\pi\xi R1(\tan\theta_1+\tan\theta_2)]}{\pi\xi(4\pi^2\xi^2\tan^2\theta_2-4\pi^2\alpha^2)} \\
&\quad\times[\exp\{-j2\pi\alpha R0\}[-j2\pi\alpha\sin(2\pi\xi R0\tan\theta_2)-2\pi\xi\tan\theta_2\cos(2\pi\xi R0\tan\theta_2)] \\
&\quad\quad-\exp\{-j2\pi\alpha R1\}[-j2\pi\alpha\sin(2\pi\xi R1\tan\theta_2)-2\pi\xi\tan\theta_2\cos(2\pi\xi R1\tan\theta_2)]].
\end{aligned}
$$

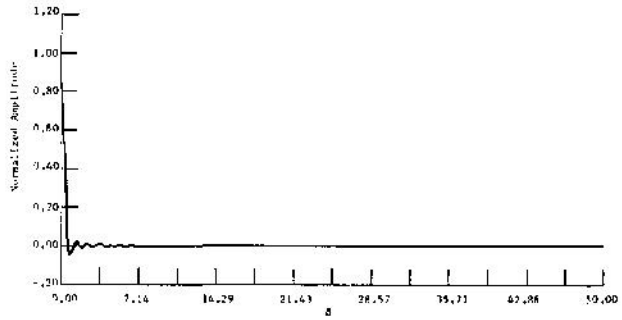

FIG. 3. The transform of the sunburst at $A=0°$; it appears similar to that of a circle, close on axis. $K=3.009$.

To rotate the coordinates, it is useful to express α and ξ in polar form,

$$\alpha_0=\beta\cos(A),$$
$$\xi_0=\beta\sin(A).$$

When the coordinates are rotated, α and ξ for each tooth are

$$\alpha_n=\beta\cos\left(A+\frac{2\pi n}{N}\right),\quad n=0,1,2,\ldots,N-1$$

$$\xi_n=\beta\sin\left(A+\frac{2\pi n}{N}\right).$$

The full transform is equal to the sum of the contributions from all of the teeth,

$$F(\alpha_0,\xi_0)$$
$$=\sum_{n=0}^{N-1}F_1\left[\alpha=\beta\cos\left(A+\frac{2\pi n}{N}\right),\ \xi=\beta\sin\left(A+\frac{2\pi n}{N}\right)\right]$$
$$+F_2\left[\alpha=\beta\cos\left(A+\frac{2\pi n}{N}\right),\ \xi=\beta\sin\left(A+\frac{2\pi n}{N}\right)\right]$$
$$+F_3\left[\alpha=\beta\cos\left(A+\frac{2\pi n}{N}\right),\ \xi=\beta\sin\left(A+\frac{2\pi n}{N}\right)\right]. \quad (5)$$

We wrote a computer program to perform the necessary coordinate transformations, summations, and iterations.

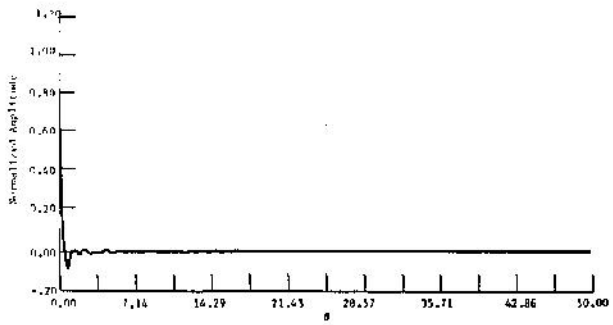

FIG. 4. The transform of the sunburst at $A=9°$; close on axis, it again appears similar to that of a circle. $K=3.009$.

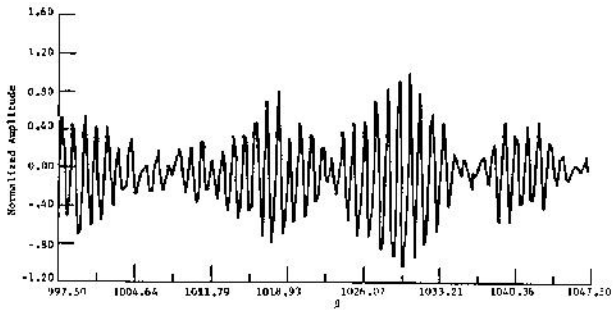

FIG. 5. At high spatial frequencies and at $A=9°$, frequency beats between the circle and sawtooth are maximum. $K=2.15\times10^{-6}$.

COMPUTER RESULTS

The sunburst aperture analyzed is shown in Fig. 2. It consists of 20 teeth whose heights are 5% of the circle radius and whose orientations are shown. The x, y coordinate system is transformed into α, ξ, respectively. Because of the symmetry of the aperture, the transform results in symmetry that is more easily shown in polar coordinates with β as the radius and A as the angle from the α axis. β can be viewed as the off-axis angle of the diffracted pattern and A is the angle in the plane of observation. All of the results shown are direct two-dimensional Fourier transforms, which correspond to the electric-field diffraction.

The sunburst aperture has an outer radius of 1 and an area of about 3.01. Each sawtooth obscuration is 0.05 high and the first tooth is at 71.6188° to the axis. The perpendiculars to the teeth consequently are at the angles

$$\phi=0.3812+18n. \quad (6)$$

The aperture is symmetric every 18°; the transform should therefore repeat every 18°.

Figure 3 shows the transform along the α axis with $A=0$, whereas Fig. 4 shows a plot with $A=9°$. β has the dimension of spatial frequency, i.e., number/length. At zero spatial frequency, the transform takes on the value of the aperture area, approximately 3.009. Because the height of each tooth is small compared to the radius of the circle, the transform for low spatial

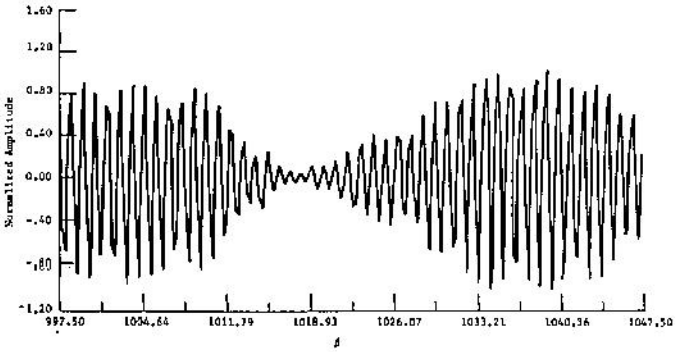

FIG. 6. At high spatial frequencies and at $A=3°$, periodicity of the beat frequency is longer. $K=3.4\times10^{-6}$.

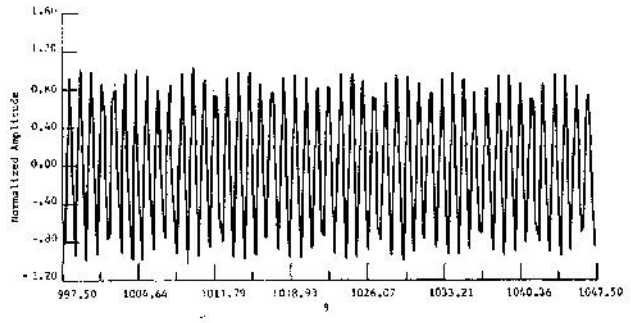

FIG. 7. At high spatial frequencies and at $A=0.3812°$, the beat frequency diminishes, whereas the transform amplitude is maximum. $K=5.3\times10^{-5}$.

frequency is very similar to that of a circle. K is the scale factor for the vertical axis of each plot.

Transforms for higher spatial frequencies are shown in Figs. 5–7. Because the 9° point lies along the direction of the peak of a sawtooth, the transform of Fig. 5 shows maximum beats of the spatial frequencies of the circle and the sawtooth. The peak amplitude is about one-third of that of an equivalent circle, at the same spatial frequency. As shown in Eq. (6), $A=0.3812°$ is perpendicular to one of the edges; Fig. 7 shows that the amplitude of the transform is about 10 times that of an equivalent circle. The small periodic modulation is caused by inadequate sampling of the function. The cross modulation between the circle and the sawtooth is a rather slow variation and is not evident because of the short length of plot.

Figures 8–12 are spatial-frequency plots in angular direction with β fixed. At high spatial frequencies, Figs. 10 to 12 show that maximum amplitude occurs at roughly 0.38°, which is perpendicular to the edge of one sawtooth. This is because far-off-axis diffraction is caused by edges and is maximum in directions perpendicular to them. Each peak is about 10 times that of an equivalent circle; the envelope decreases to about 1/30 as much at 9°. Integration of power at constant β yields a total approximately equal to that of a circle. Although the power spectral distribution is markedly different between a circle and the sunburst aperture, the integrated power around a constant off-axis angle β appears to be equal for the two apertures.

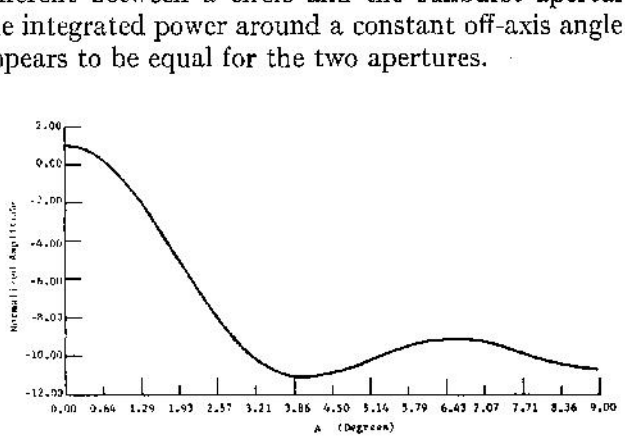

FIG. 8. Sunburst transform close on axis in the angular direction. $\beta=10$. $K=8.3\times10^{-4}$.

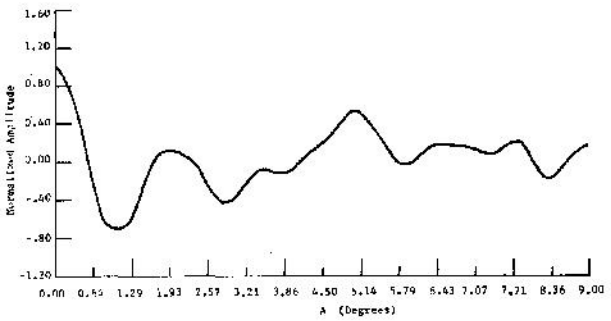

FIG. 9. Sunburst transform along angular direction at $\beta=100.107$. $K=4.174\times10^{-4}$.

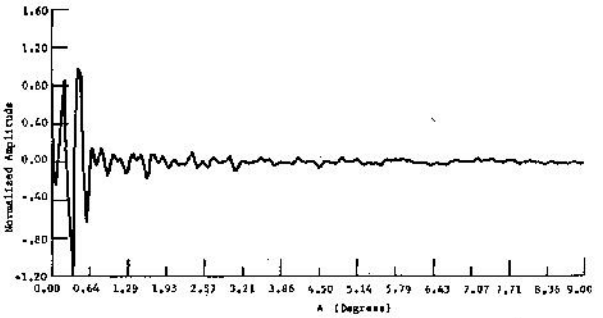

FIG. 10. At $\beta=1001.07$, the sunburst transform shows peaks around $A=0.38°$, which is perpendicular to an edge. $K=4.9\times10^{-5}$.

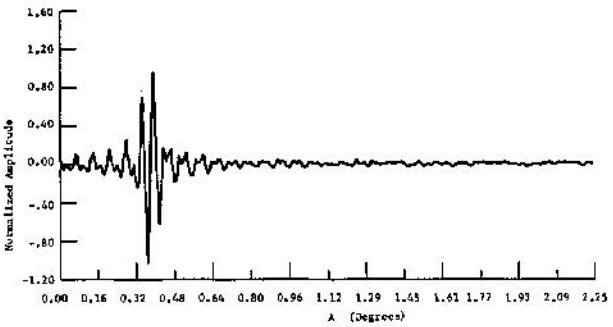

FIG. 11. As β increases to 5241, the magnitude of the transform decreases but the maximum remains at 0.38°. $K=8.5\times10^{-6}$.

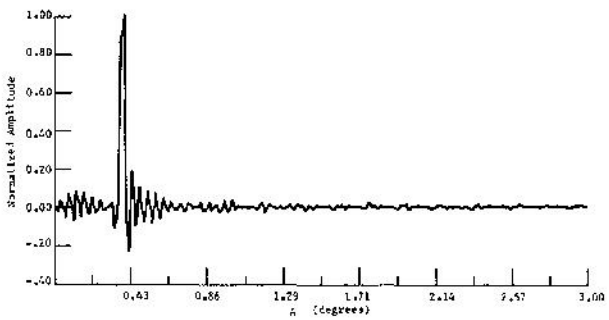

FIG. 12. At $\beta=16000$, the transform maxima remain at angles perpendicular to the edges. $K=1.212\times10^{-6}$.

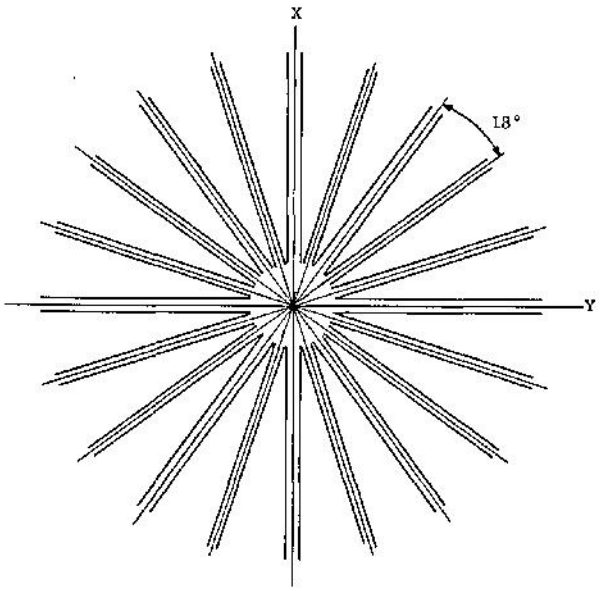

FIG. 13. Sketch of diffraction pattern of sunburst aperture with 20 teeth.

CONCLUSION

Figure 13 is a sketch of the diffraction pattern of a sunburst aperture. At high off-axis angles, the pattern exhibits bright arms, one for each straight edge. Because, in general, sensors are designed with detectors in the back focal plane of an optical imaging element, apodizing apertures in the system would result in controlled diffraction patterns in the focal plane. Replacing a circular aperture with a sunburst could improve diffraction rejection if the aperture were oriented correctly and the stray source were small in angular extent. For an extended source, the advantage decreases, as a result of the smearing of the diffracted pattern. The convolution of the diffracted pattern with the extended-source function serves to smear out the bright arms into the field of view of the system.

Other effective shapes of apertures are squares, rectangles, diamonds, etc. Selection of an aperture shape depends on the parameters of the field of view, the effective aperture size, and the size of the source. For extended sources, aperture shaping becomes useless. A more-effective means is then the use of a series of correctly designed stops and transmission filters.

REFERENCES

*Study supported by the U. S. Air Force/SAMSO under contract No. F04701-71-C-0147.

[1]P. Jacquinot and B. Roizen-Dossier, in *Progress in Optics III*, edited by E. Wolf (North–Holland, Amsterdam, 1964), Ch. II.
[2]J. D. Purcell and M. J. Koomen, *Coronograph with Improved Scattered-Light Properties*, The Report of NRL Progress, 1962 (U. S. Government Printing Office, Washington, D. C., 1962).
[3]G. Newkirk and D. Bohlin, Appl. Opt. **2**, 131 (1963).
[4]J. W. Goodman, *Introduction to Fourier Optics* (McGraw–Hill, New York, 1968), Chs. 4 and 5.